Analysis of the BCAL Hall-B Beam test

GlueX-doc-804-v5

Blake Leverington
Regina, Saskatchewan, Canada

Abstract

A beam test of the 4m prototype module for the GlueX barrel calorimeter (BCAL) was carried out in Hall B at the Thomas Jefferson National Accelerator Facility (Jefferson Lab) with the objective of measuring the energy, timing and position resolution of the module. The data were collected in September 2006. Preliminary analysis results of the timing and energy resolution will be shown here.

1. Introduction

...

2. Experimental Details

2.1. *Module Construction*

The prototype module for the GlueX Barrel Calorimeter (BCAL) is constructed of alternating layers of pure, grooved lead and blue Poli-Hi-Tech scintillating fibres bonded together with Bicron-600 optical epoxy. Construction took place at the University of Alberta. Construction and the internal geometry of the BCAL can be seen in Figure 1.

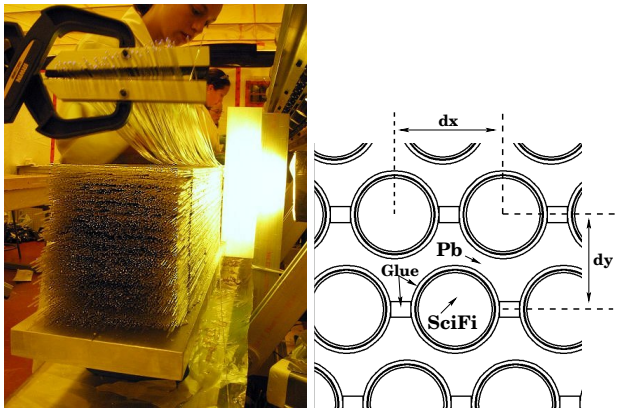

Fig. 1. Construction of the module.

2.2. *Alcove*

The module was placed in the down stream alcove of Hall B at Jefferson Lab. The use of a remote controlled cart allowed for the module to be rotated to various angles with respect to the photon beam. A hall access was needed to change the lateral position of the module with respect to the beam. The smaller dimensions of the alcove limited the number of angles and positions the module could be placed in but a length scan from -100 cm to +25 cm perpendicular to the beam was able to be performed along with multiple positions at shallow angles with respect to the beam. Only data where the module was perpendicular to the beam are addressed in this note.

Email address: leverinb@uregina.ca (Blake Leverington).

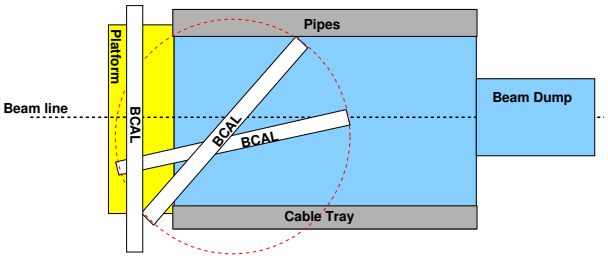

Fig. 2. Diagram of the Hall-B downstream alcove with possible placements of the BCAL module.

2.3. *The Hall-B Photon Beam and Tagger*

The bremsstrahlung photon beam in Hall B provided a spectrum of photons from 150 MeV up to 650 MeV produced by the 675 MeV electron beam from CEBAF incident on a radiator. The electron beam current was 1 nA. The scattered electrons are tagged and provide timing and momentum information for the photons. The tagger provides the momentum information from 384 individual scintillator paddles, called E-counters, with a photo-tube on each end. They are arranged so that they each cover constant momentum intervals of $0.003E_o$. Each counter optically overlaps its adjacent neighbour by 1/3 creating 767 individual photon energy bins providing an energy resolution of $0.001E_o$. The timing information is provided by 61 individual scintillator blocks, called T-counters, with phototubes attached at both ends. The T-counters are in two groups. The first 19 narrower counters cover 75% to 90% of the incident electron energy range and the remaining 42 counters cover the 20% to 75% range (1). The trigger is formed from the Master OR from the tagger of the T-counters and an OR signal from the North and South of the BCAL module. On average, the event rate was around 1 to 4 kHz for the duration of the beam test. The beam was collimated with a 2.6mm collimator giving a beam spot size on the BCAL module of 2cm in diameter.

2.4. *Readout and Electronics*

The module was segmented into 18 $3.8cm \times 3.8cm (1.5'' \times 1.5'')$ cells with 6 rows in depth with respect to the beam and 3 columns in width. They were then numbered 1 through 18. The readout scheme can be seen in Figure 4. Square light guides with a 45 degree mirrored surface channelled the light from the fibres to PMTs on the left and right end of the BCAL, labelled South and North respectively. Silicon sheets approximately 2.5 mm thick were used to interface the light guides with the BCAL and the PMTs. Everything was then enclosed in a steel box to maintain light-tightness. The light boxes and PMT's can be seen in 3. The first three rows are readout using XP2020 photomultiplier tubes because of their better timing characteristics and most of the energy is deposited in the first 12 cm of the BCAL. The last three rows are readout using Burle 8575 tubes.

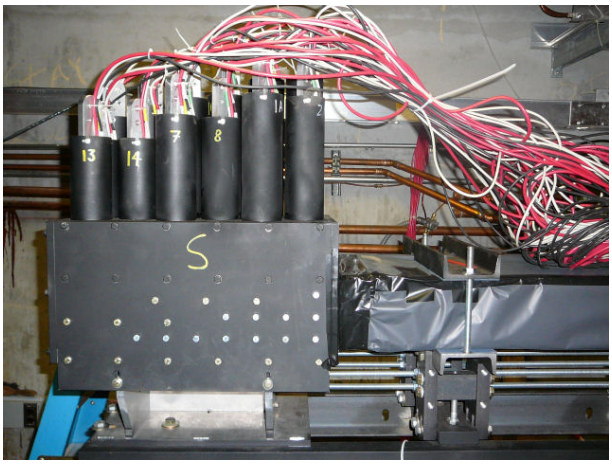

Fig. 3. The black box encloses the 18 light guides and PMTs with cables attached for the South end of the BCAL module and is similar to the North end. The BCAL Pb/Sci-Fi matrix is wrapped in Tevlar on the right and pressed against the light guides coupled with a silicone cookie.

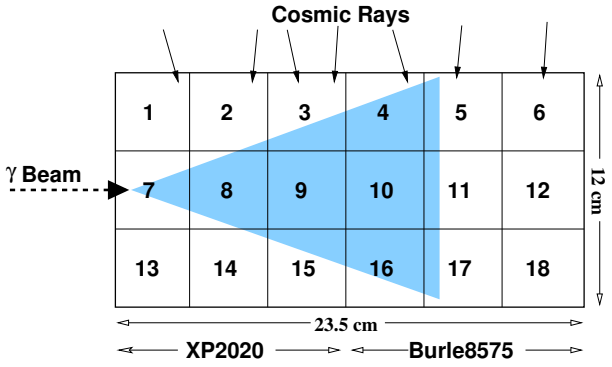

Fig. 4. The segmentation and readout for the BCAL module.

The bases for the PMTs were designed with dual BNC outputs on the anode. One signal was sent to a CAEN C 207 (equivalent leading edge) discriminator. An F1 TDC was used. The sum of the discriminator output was sent to a second discriminator and was required to reach a minimum threshold such that at least 4 PMTS each from the North and South end of the BCAL must fire. The effect of changing this threshold (number of PMTs that fire) will also be studied. The OR of the BCAL end sums AND the Master OR signal of the tagger established the trigger for the BCAL beam test.

2.5. *Goals*

The design of the BCAL is very similar to the KLOE electromagnetic calorimeter which had a reported energy resolution of $5.7\%/\sqrt{E(GeV)}$ plus a negligible constant term (it is never stated what the value actually is is. See Fig. 5) and a timing resolution of 54 ps/$\sqrt{E(GeV)}\oplus$ 50 ps (2). GlueX expects similar resolutions for the BCAL though different fibres and readout will be used as well as GlueX is a fixed target experiment unlike KLOE which was a collider experiment.

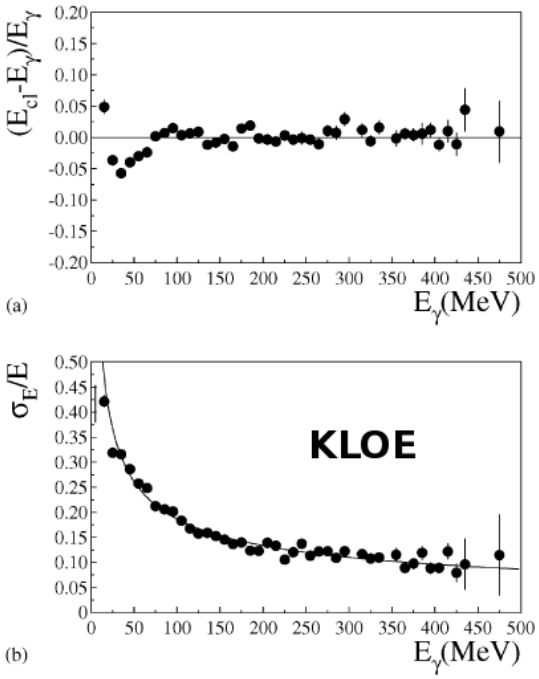

Fig. 20. $(E_{cl} - E_\gamma)/E_\gamma$ (a) and resolution (b) vs. E_γ for $e^+e^-\gamma$ events. The fit gives $\sigma(E)/E = 5.7\%/\sqrt{E(\mathrm{GeV})}$.

Fig. 5. This is the energy resolution plot taken from (2)(Fig.20)

3. Energy Analysis

3.1. *Gain Balancing*

With the BCAL segmented into 18 cells on the North and South sides, 36 PMTs are needed and each has its own applied high voltage. Therefore 36 individual gains must balance in order to have identical ADC spectra from each cell for a given energy deposition. Three different methods have been used to determine what the relative gain of each of the cells are. In one method a minimization algorithm was used to adjust each of the gains to minimize the width of the parameter D defined as

$$D = \frac{E_{BCAL} - E_{BEAM} * C}{E_{BEAM}} \quad (1)$$

where E_{BCAL} is the reconstructed energy in the BCAL module and E_{BEAM} is the energy measure in the tagger. C is a constant derived from Monte Carlo data to account for energy losses out the sides and back of the module. We attempt to reconstruct the deposited energy in the module not the tagger energy. A value of $C = 0.95$ was found from a Monte Carlo simulation. The width of this distribution, σ_D, is also the energy resolution, σ_E/E.

The minimization technique accounts for the inter-PMT calibration. The overall calibration to relate ADC values to energy is determined by applying the inter-PMT calibration in determining the geometric mean of the sum of the North ADCs and the sum of the South ADCs and comparing this the tagger energy as seen in Figure 7. The linear fit provides the slope and some offset most likely due to some minor error in the pedestal subtraction. In addition, one can see that the data points are not quite linear and fall below the fit at the higher energies. This is most likely due to increased leakage out of the module at higher energies. However, the linear fit takes care of most of the leakage in the reconstructed BCAL energy. Simulations show the reduction in photon energy sampling due to leakage which can be seen in Figure 6. The losses scale nearly linearly above 200 MeV.

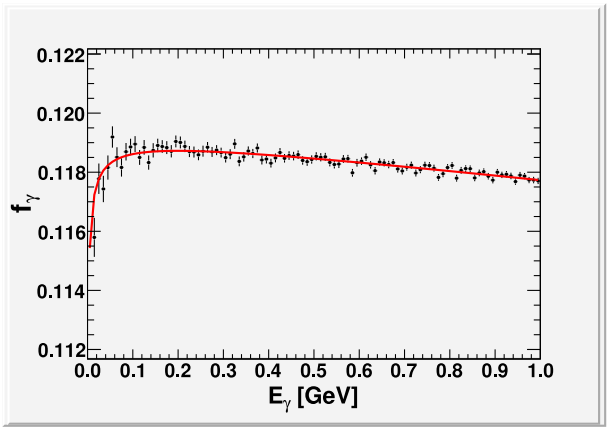

Fig. 6. The photon energy sampling fraction, f_γ, from simulation.

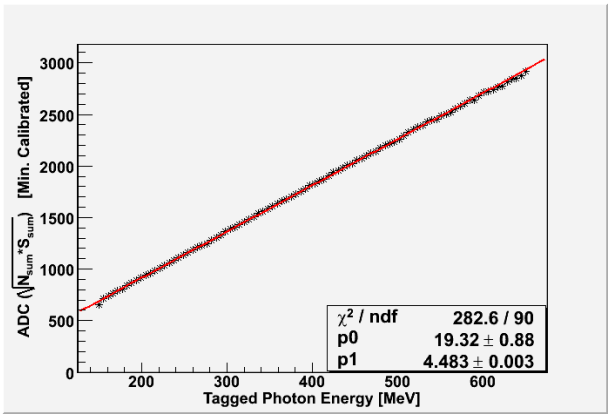

Fig. 7. A plot of the ADC geometric mean (minimization calibration) vs. tagger energy with a linear fit.

Figure 7 is produced by projecting the ADC vs Energy spectra to a 2-D histogram and using the FitSlicesY function in CERN's ROOT package to fit a Gaussian function to each slice. Each point is the mean of the Gaussian fit. The sigma of the distribution divided by the mean, σ_{ADC}/ADC, also gives the energy resolution of the BCAL, σ_E/E.

In a second method the same Monte Carlo was used to determine the energy deposited in each cell. The photon energy spectra from the tagger was used as an input for the simulation. Fitting the peaks of each distribution allowed us to find an energy calibration for each cell. This method will not be used further in this analysis as the beam test will be used to validate the Monte Carlo itself.

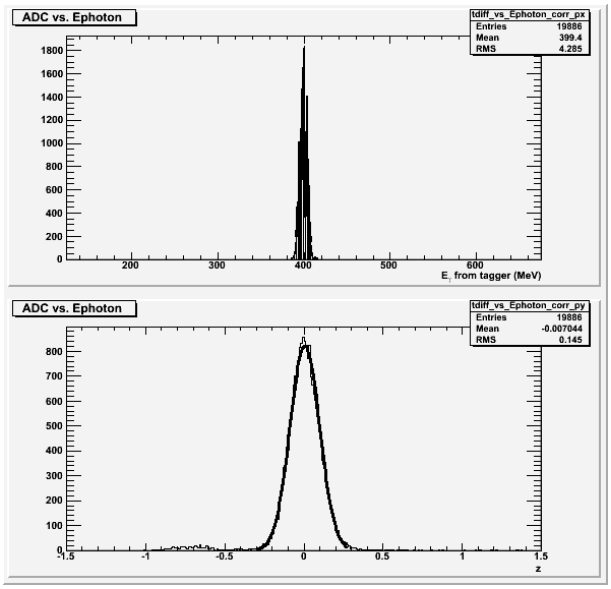

Fig. 8. The ADC geometric mean spectra for the tagger energy distribution given in the top panel.

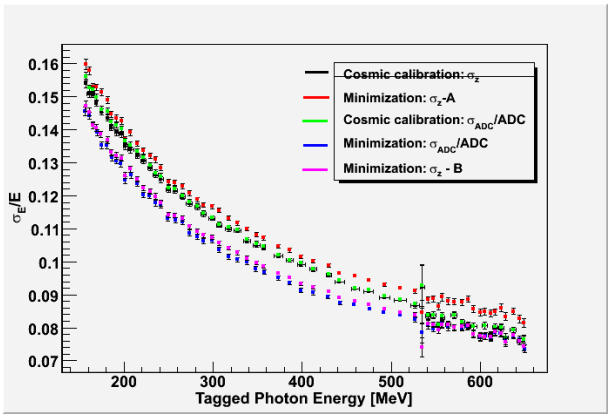

Fig. 9. A plot of energy resolution using both z-minimization and cosmic calibrations.

The third method was to use cosmic ray data collected during the beam test to gain balance each of the cell. A minimum ionizing particle will deposit the same amount of energy in each of the cells and should produce the same ADC response from each cell. Details of how the cosmic data were used to balance the gains are given in Gluex-doc-834 (4). Deviations of each cell from unity can then be corrected for. As seen in Figure 9, the comic calibration and z-minimization both perform almost equally well. It is possible that both methods may still be improved to find better calibration constants for each PMT.

3.2. *Energy resolution*

The energy resolution is expressed in the form

$$\frac{\sigma_E}{E} = \frac{a}{\sqrt{E(GeV)}} \oplus b \oplus \frac{c}{E(GeV)} \qquad (2)$$

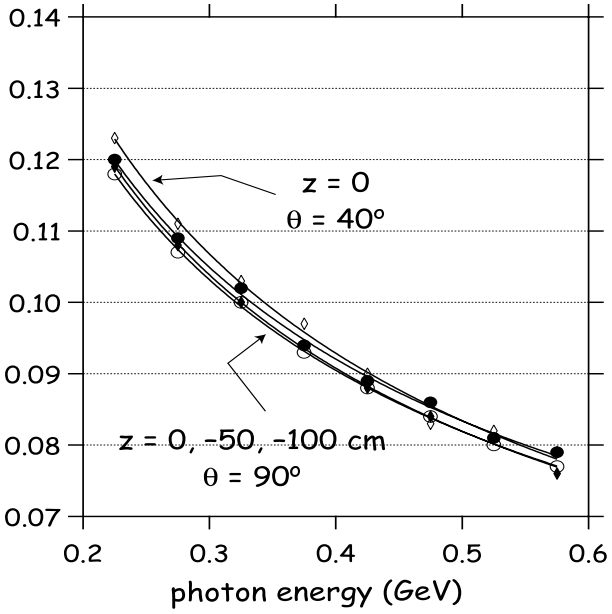

Fig. 10. The energy resolution for three z-positions.

The $a/\sqrt{E}$ term measures the sampling fluctuations and photoelectron statistics which both contribute to the resolution. It will be referred to as the sampling term. The $1/\sqrt{E}$ dependence is expected from the fact that the fluctuations are proportional to the number of particle tracks, n, that cross the active material, where n has a Poisson distribution with a variance $\sqrt{n}$. Since the energy of a shower is proportional to n, the sampling fluctuations contribution to the resolution σ_E/E is $\propto 1/\sqrt{E}$. KLOE (3) determined the photon statistics from the light yield of their calorimeter to contribute $1.6\%/\sqrt{E}$ and determined it contribute very little to the resolution. It is the sampling fluctuations that dominate the resolution. Since this is the case there should be little effect of z-position on the energy resolution as attenuation only affects the light yield at the module ends. This can be seen in the beam test data shown in Figure 10.

Because the sampling frequency (how many layers or fibres the shower encounters) decreases with decreasing $sin(\theta)$, where θ equal to 90^o is defined as being perpendicular to the 4 metre length of the module and 0^o is parallel, the sampling term of the resolution will be degraded by a factor

$$\frac{\sigma_{samp}}{E} \propto \frac{1}{\sqrt{sin(\theta)}} \qquad (3)$$

Also as one starts to go to angles less than 40^0 increasing portions of the shower are lost outside of the module.

The constant term b is from mechanical imperfections, material defects, shower leakage, cell to cell calibration, uniformity of response and stability with time. At incident photon angles beginning around 40 degrees and lower shower leakage increases and will cause the floor term to begin to increase.

The noise term c/E is from electronics noise and pileup in high rate environments. This term will dominate at the

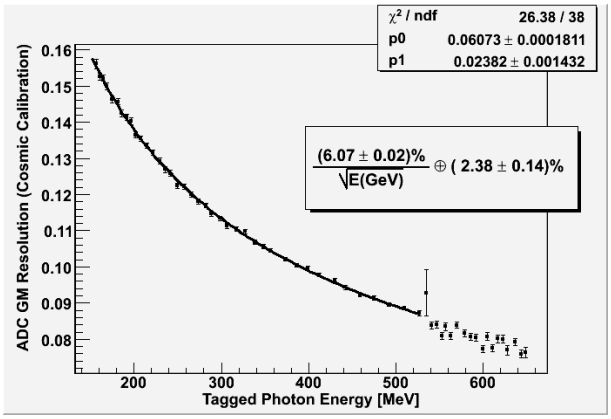

Fig. 11. The energy resolution using cosmic ray calibration for each cell

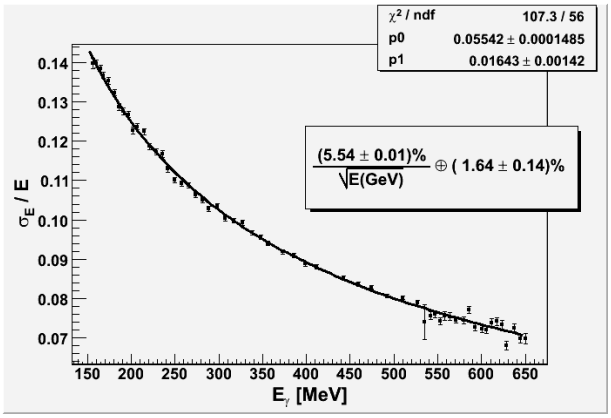

Fig. 12. The energy resolution using the minimization algorithm calibration.

lower energies but has not been seen to contribute in the beam test as the rates were quite low and the signal to noise ratio was quite large. Fits to the beam test data including this term produce almost identical sampling and constant terms with values for c on the order of 2×10^{-5}.

The fit from Figure 11 gives an energy resolution for the BCAL of

$$\frac{\sigma_E}{E} = \frac{6.1\%}{\sqrt{E(GeV)}} \oplus 2.4\% \tag{4}$$

and the fit in Figure 12 gives an energy resolution of

$$\frac{\sigma_E}{E} = \frac{5.54\%}{\sqrt{E(GeV)}} \oplus 1.64\%. \tag{5}$$

The effect of angle on the energy resolution coefficients can be seen in Figures 13, a varies as a function of $1/\sqrt{sin\theta}$ and in 14, which varies as a function of $1/\sqrt{sin\theta + \theta_{min}}$, where the angle at which the floor term is minimum is $90^o - \theta_{min}$. This is the angle at which there is little or no loss due to leakage out the back side of the module as well as little shower leakage outside the front of the module. Essentially, this is the most efficient angle for the BCal.

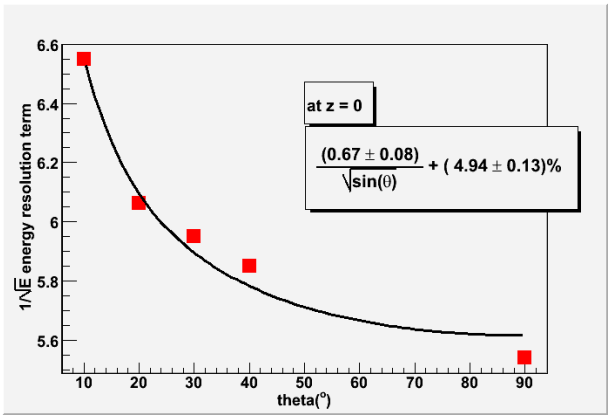

Fig. 13. The energy resolution coefficient, a, as a function of angle.

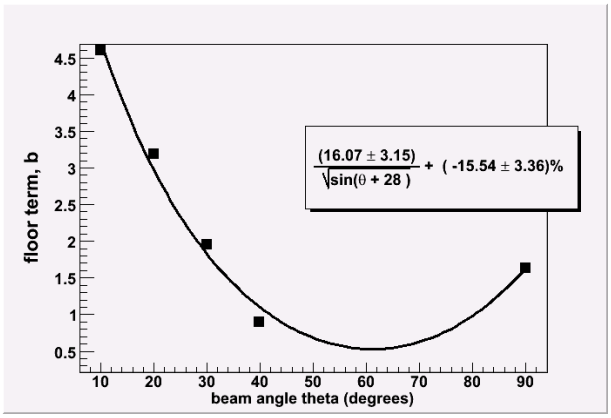

Fig. 14. The energy resolution coefficient, b, as a function of angle.

4. Time and Position Resolution

4.1. *Time walk corrections*

Because leading edge discriminators were used, the timing had a dependence on pulse height which required a time walk correction. A plot of ADC versus TDC for cell 8 can be seen in Figure 15. A $p0/\sqrt{ADC} + p1$ fit was applied as the time delay due to signal amplitude in leading edge discriminators follows this form. $p1$ is some constant term indicating the timing offset of the particular BCAL cell from the tagger Master OR (MOR) timing signal with a value of approximately $530ns$. p0 also varies depending on the particular BCAL cell but has a nominal value of $30 - 40ns * \sqrt{ADCchannel}$. Similar fits have been done for all cells but the quality of the fit is poor for the back cells, specifically cells 6 and 18 where the statistics are low, very little energy is deposited and the fluctuations are large. The corrected TDC distribution for South 8 can be seen in Figure 16. Early analysis of the timing data focused mainly on cell 7,8,9 and 10 where most of the energy, nearly 90% (see Fig. 22, was deposited. ADC values below channel 350 were cut, in the case of S8, due to the resulting assymetry from the walk correction at low ADC values which cause distortions in the time difference resolution. This results in a few events being sacrificed at the lower energies but

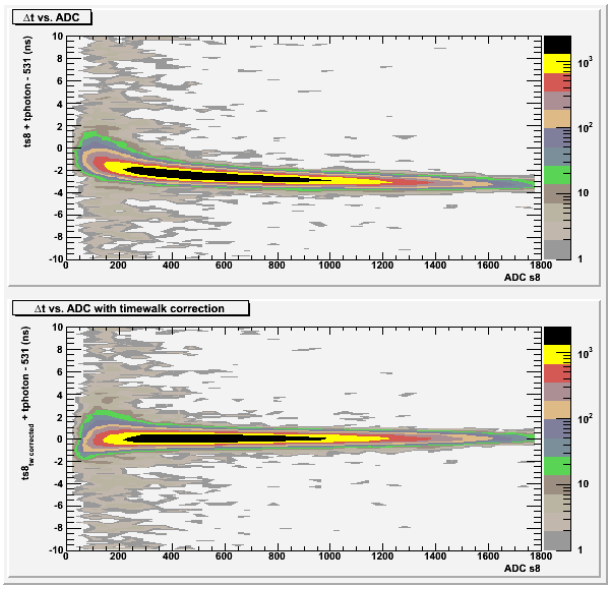

Fig. 15. ADC vs. TDC for cell South 8. The uncorrected time walk is seen in the top plot. The bottom plot shows the corrected time.

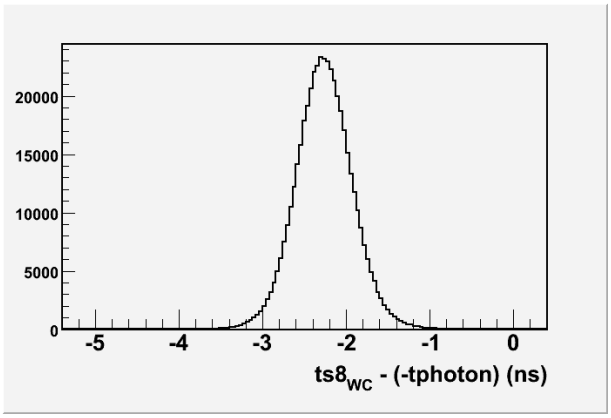

Fig. 16. TDC distribution for South 8 corrected for time walk

a much improved time difference resolution over the whole tagger spectrum.

4.2. *Timing resolution*

The distribution of the mean time using the average of the North and South TDCs over the entire tagger energy spectrum for cell 8 can be seen in Figure 17. The timing from the tagger, tphoton, has been used as the reference time for the BCAL which has a contribution to the constant term in the resolution of ∼120 ps (see Fig.26). The distribution for the time difference of cell 8, South minus North, $(ts8 - tn8)$, can seen in Figure 18. The mean value is the offset $(ts8_o - tn8_o)$ from the time difference being zero at the middle of the module. A plot of the timing resolution of cell 8 can be seen in Figure 21. The width of the photon beam (1.8 cm) will contribute 113 ps to the time difference resolution where the speed of light in the BCAL is measured to be 16 cm/ns.

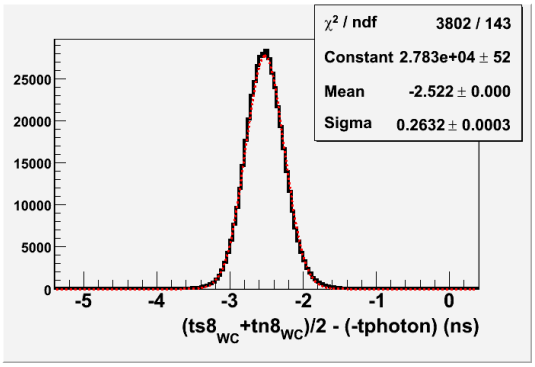

Fig. 17. The mean timer distribution of cell 8 corrected for time walk and referenced with the tagger

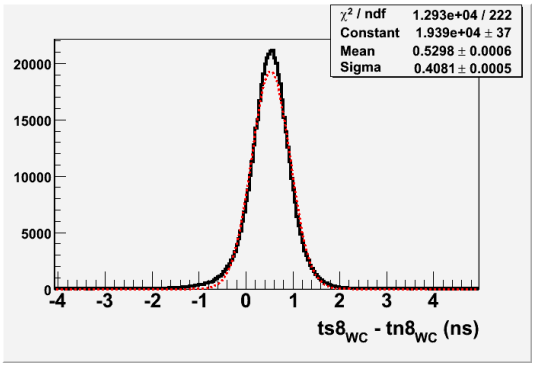

Fig. 18. The distribution of the difference between North 8 and South 8

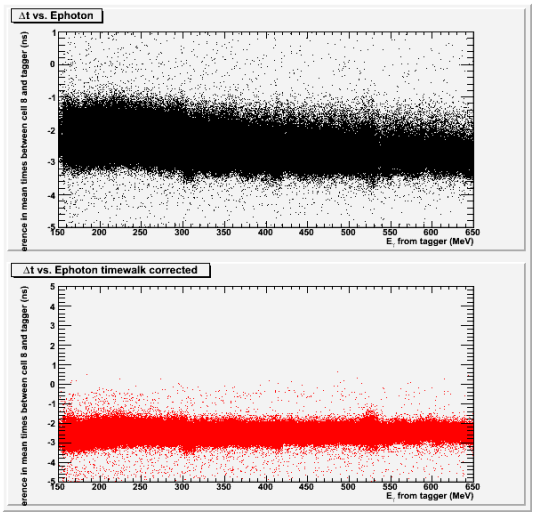

Fig. 19. (tn8+ts8)/2 - (-tphoton) vs. Tagger Energy(MeV for Cell 8). The top plot is before time walk corrections. The bottom plot is after walk corrections.

Looking at Figure 20, a single mean value for the offset of $(ts8 + tn8)/2 - (t_{tagger})$ is expected. However, there is a deviation from the expected value by over 100 ps at some energies. t_{tagger} is the reference time from the tagger.

Subtracting the contribution of the tagger to the resolution, 113 ps, we are left with a resolution for the mean timer,$\sigma((ts8 + tn8)/2 - (t_{tagger}))$, of cell 8 equal to

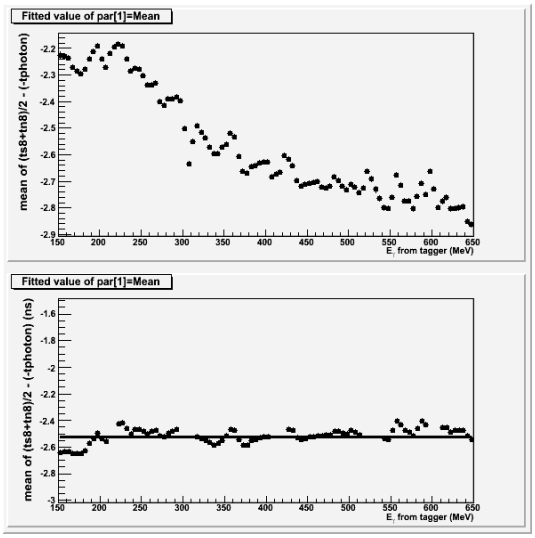

Fig. 20. The mean of the distribution in Figure 19 The top plot is before time walk corrections. The bottom plot is after corrections.

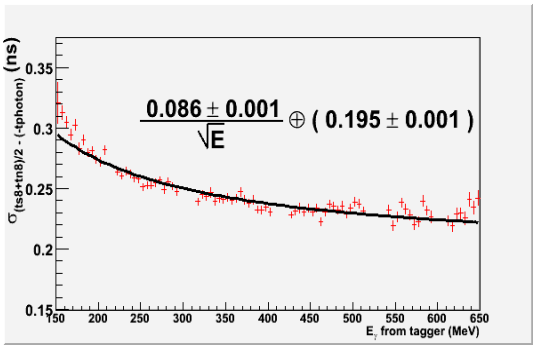

Fig. 21. Timing resolution from fitting the slices of Figure 19

$$\sigma_{t8_{MT}} = \frac{86ps}{\sqrt{E(GeV)}} \oplus 159ps \tag{6}$$

where $\oplus$ indicates addition in quadrature. The resolution of the mean timer of cell 7 is

$$\sigma_{t7_{MT}} = \frac{61ps}{\sqrt{E(GeV)}} \oplus 176ps \tag{7}$$

Since this is the result for the sum of 2 detectors the resolution for reading out one end will be $\sigma_{t7_{MT}} * \sqrt{2}$. The resolutions for one end of cell 8 and cell 7 respectively are then

$$\sigma_{t8} = \frac{122ps}{\sqrt{E(GeV)}} \oplus 225ps \tag{8}$$

$$\sigma_{t7} = \frac{86ps}{\sqrt{E(GeV)}} \oplus 249ps \tag{9}$$

Weighting the time of each cell by $1/\sigma_i^2$ the time for a cluster is equal to

$$t_{cl} = \frac{\sum_i \frac{t_{MT}(i)}{\sigma^2_{MT}(i)}}{\sum_i \frac{1}{\sigma^2_{MT}(i)}} \tag{10}$$

where there are i cells in the cluster. For now, just adding cells 7 and 8 (4 PMTs) together gives a resolution of

$$\sigma_{t7\&8} = \frac{60ps}{\sqrt{E(GeV)}} \oplus 187ps \tag{11}$$

Subtracting the contribution from the tagger then gives

$$\sigma_{t7\&8} = \frac{60ps}{\sqrt{E(GeV)}} \oplus 149ps \tag{12}$$

One also has to be careful when making cuts on the ADC value of each cell. This has an effect mostly on the energy dependent term of the resolution, especially for the cells which do not see much energy like cells 9 and 10. Here, the fluctuations are large and the statistics are low for low energy photons. An ADC cut which is too small or too large will affect the resolution fit.

4.3. *Further timing study*

Further study of the timing resolution resulted in a better understanding of extracting the timing resolution. Firstly, time walk corrections must be done well. A small issue with the tagger timing was causing problems when trying to do walk corrections due to the fact that the t-counters of the tagger corresponded to a given energy range as they are physically positioned in front of a set of e-counters. When using the timing information of the tagger as a reference for a single channel of the BCAL to perform the walk correction, there resulted an energy dependence on the time. This issue was corrected and the walk correction are now much more satisfactory. Secondly, there should be no bias when making an ADC cut. When adding a cell to the cluster, the only criteria should be that the ADC signal for that event does not lie within the pedestal. A cut of ADC¿5 channels usually satisfies this. A cluster is defined as the energy weighted sum of the times of each cell expressed as

$$\bar{T} = \frac{1}{2}\frac{\sum_i t'_{N,i}E_{N,i} + t'_{S,i}E_{S,i}}{\sum_i (E_{N,i} + E_{S,i})} \tag{13}$$

$$\Delta T = \frac{1}{2}\left(\frac{\sum_i T_{N,i}E_{N,i}}{\sum_i E_{N,i}} - \frac{\sum_i T_{S,i}E_{S,i}}{\sum_i E_{S,i}}\right) \tag{14}$$

The t' indicates that the time is referenced with another time signal, usually the tagger. For efficiency only cells 7,8,9 and 10 were included in the cluster as they contain 85-90% of the shower energy (see Figure 22). To be included in the cluster it was required that the North and South end of the cell both have ADC signals greater than 5 channels. This corresponds to $\tilde{1}$ MeV of energy deposited in the BCAL or $\tilde{0}.12$ MeV deposited in the fibres. The mean time of the cluster, $\bar{T}$ or the time difference, ΔT, was then calculated and the sigma of the distributions then found. An example of the time difference distribution is seen in Figure 23. The time difference resolution is seen in Figure (24). The constant term is a result of some residual calorimeter miscalibrations, but some of it is also due to the finite width in

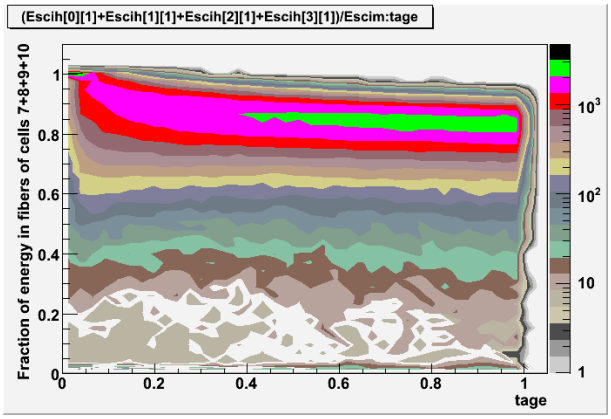

Fig. 22. From Monte Carlo: The fraction of energy deposited in the fibres of cells 7,8,9 and 10.

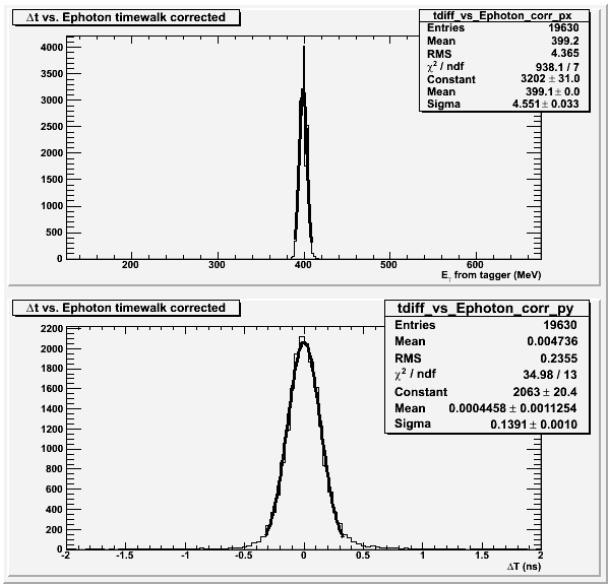

Fig. 23. An example of the time difference distribution for t-counter 28

z of the beam which will contribute to the time difference resolution. With the beam width $l \sim 1.8$ cm the spread contributes $ln/c\sqrt{12} = 28ps$ where $n = 1.6$ is the index of refraction of the fibers. Adding this in quadrature contributes little to the constant floor term. The time difference resolution of the BCAL is then found to be

$$\sigma_{\Delta T} = \frac{74ps}{\sqrt{E(GeV)}} \oplus 33ps \tag{15}$$

The mean time resolution, $\sigma_{\bar{T}}$, seen in Figure 25, shows a similar energy dependent term but a much higher floor term. One contributor to the floor term is the tagger. The counter-to-counter timing resolution is seen in Figure 26. T-counter ID=1 corresponds to about 650 MeV and T-counter ID = 59 corresponds to about 150 MeV. One can see that there are a few t-counters which were not operating correctly and were removed from Figure 25. Further work will subtract the resolution of each individual t-counter from the BCAL resolution.An example of the mean time

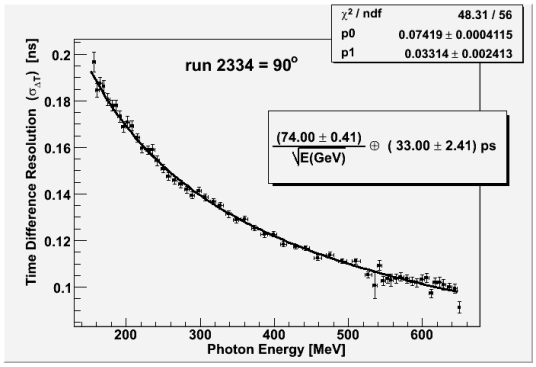

Fig. 24. The time difference resolution, $\sigma_{\Delta T}$, as a function of energy.

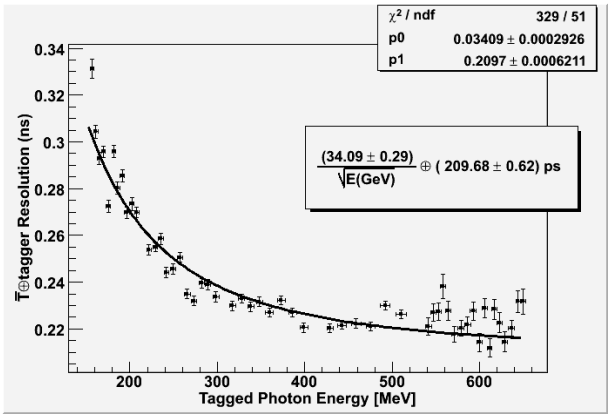

Fig. 25. The mean time resolution, $\sigma_{\bar{T}}$, without the tagger resolution extracted.

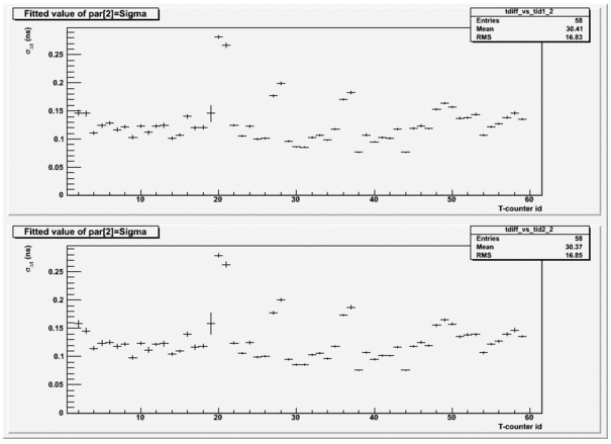

Fig. 26. The resolution of the time difference between adjacent t–counters of the Hall-B tagger.

distribution can be seen in Figure 27. The curve in Figure 25 is a fit yielding

$$\sigma_{\bar{t}} = \frac{34ps}{\sqrt{E(GeV)}} \oplus 210ps \tag{16}$$

gives the energy dependent term of the mean time resolution. The miscalibration, tagger resolution, shower spread and other contributions must still be accounted for to determine the correct constant floor term.

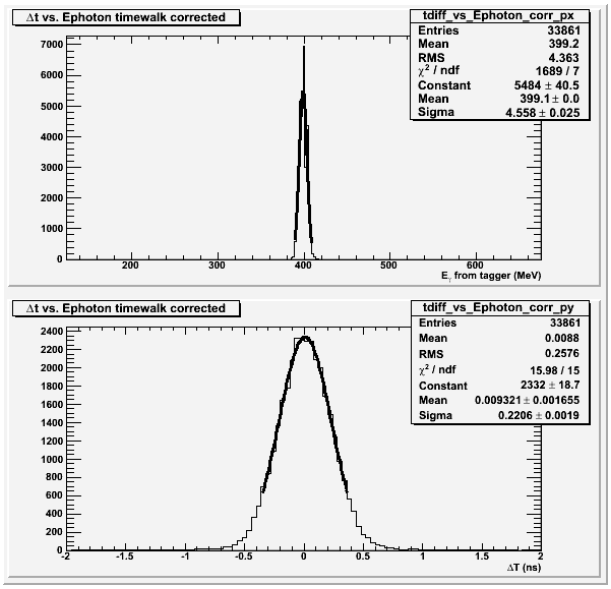

Fig. 27. An example of a $\bar{T}$ distribution corresponding to t-counter 28.

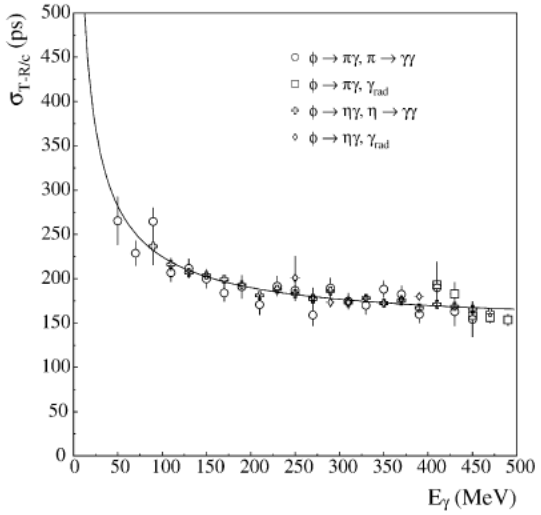

Fig. 32. Time resolution as a function of E_γ for ϕ radiative decays.

Fig. 28. Figure taken from (2).

For completeness I've included KLOE's time resolution plot (2), seen as Figure 28. The fit yields

$$\sigma_t = \frac{54ps}{\sqrt{E(GeV)}} \oplus 140ps. \tag{17}$$

The floor term still includes residual miscalibrations and spread due to time spread of the bunch length.

References

[1] Sober, D.I. et al. The bremsstrahlung tagged photon beam in Hall B at JLab 2000, Nucl. Instrum. Meth. A440, 263-284

[2] Andolfini, M. et al., The KLOE electromagnetic calorimeter, 2002, Nucl. Instrum. Meth. A482, 364-386.

[3] Antonelli, A. et al., Construction and performance of the lead-scintillating fiber calorimeter prototypes for the KLOE detector, 1995, Nucl. Instrum. Meth. A354, 352-363.

[4] Dzierba, A. Calibrating BCAL with Cosmic Rays Gluex-doc-834-v1 June 29, 2007